Ab Initio Study of the Mechanism for the Thermal Decomposition of the Phenoxy Radical

Ruifeng Liu, Keiji Morokuma,* Alexander M. Mebel, and M. C. Lin*

Department of Chemistry and Cherry L. Emerson Center for Scientific Computation, Emory University, Atlanta, Georgia 30322

Received: December 1, 1995; In Final Form: February 14, 1996[⊗]

Various *ab initio* methods have been applied to the studies of the molecular structure and energetics for the low-lying electronic states of the phenoxy radical and of the mechanism of its thermal decomposition. The calculations confirm the decomposition mechanism I (Scheme 1) suggested earlier from experimental consideration. It involves the formation of the bicyclic intermediate E2 followed by α-CC bond cleavage to produce E3 and the elimination of the CO group from the latter leading to the main reaction products, C_5H_5 + CO. The rate-determining step is E2 → E3 with transition state T2. The activation energy, 52 kcal/mol, at our best G2M(rcc,MP2) level, is 8 kcal/mol higher than the value derived from experiment. A multistep RRKM calculation has been performed for the decomposition reaction. The theoretical rate constants agree well with the experimental results at lower temperatures (T < 1200 K) but deviate from experiment above 1300 K. Plausible reasons for the deviation have been discussed. On the basis of state-specific and state-averaged CASSCF calculations, the observed electronic transitions for the phenoxy radical have been assigned.

I. Introduction

It is expected that the fuels of the future will increasingly contain more aromatic compounds because of the change in fuel sources such as coals and shell oils and partly because of the greater use of aromatic compounds as additives due to their high octane values.[1] The phenoxy radical is an important intermediate in the combustion of many aromatic compounds.[2−8] It and its substituted derivatives are also postulated to be the intermediates in the reduction of flavoproteins,[8] in the light-induced reactions involving green plant photosynthesis,[9] and in the phenol-inhibited oxidation of hydrocarbons.[3] Due to its prototype nature, the phenoxy radical has been the subject of many diverse investigations. Experimental[10−16] and theoretical[16−19] studies on the optical absorption spectrum have indicated the presence of several low-lying excited electronic states. Measurements of the ESR hyperfine coupling (hfc) constants[20−25] and related theoretical calculations[26−30] of spin density distribution indicate that the unpaired electron is significantly delocalized from the oxygen atom onto the carbon ring π system, suggesting[25] that the CO bond may resemble the double bond typical of a carbonyl group in a closed shell system. Resonance Raman spectroscopy has been applied to gain information about molecular structure and vibrations,[31−36] and kinetic as well as dynamic studies have been carried out to investigate the rate and activation barrier of thermal decomposition.[5,6,37−39]

Many mechanistic details of the thermal decomposition of this radical remain unclear. The primary products of the thermal decomposition were found to be cyclopentadiene radical and carbon monoxide.[5,37−39] Two mechanisms[37,39] were proposed to explain the products; mechanism I in Scheme 1 involves forming a fused bicyclic cyclopropanone intermediate followed by breaking a CC bond of the three-membered ring and subsequently losing carbon monoxide. The other, mechanism II, is a direct cleavage of the α-CC bond of the benzene ring followed by cyclization to form a five-membered ring intermediate and a subsequent loss of carbon monoxide. On the basis of the results of kinetics studies and thermochemistry considerations, mechanism I is preferred.[37,39]

SCHEME 1

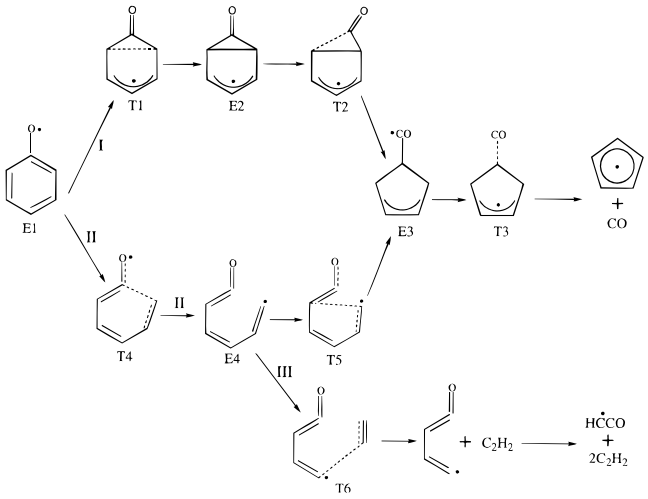

While the present manuscript was in preparation, Olivella *et al.*[40] reported a theoretical study on the thermal decomposition of C_6H_5O using *ab initio* CASPT2 and CASSCF methods. They showed that the reaction is dominated by mechanism I. The calculated activation energy, 53.9 kcal/mol at their best level, is about 10 kcal/mol higher than the value derived from experiment.[5] Olivella *et al.*[40] used the transition state theory approach to compute the rate constant for the unimolecular decomposition of the phenoxy radical. The theoretical preexponential A factor was found to be substantially larger than the experimental values.[5] While the CASPT2 method used by Olivella and co-workers is qualitatively reliable, the 6-31G-(d,p) basis set may not be sufficient to provide quantitative accuracy. Therefore, we report the results of more accurate *ab initio* calculations of the potential energy surface of the thermal decomposition of C_6H_5O. The computed energies and molecular parameters are employed for multistep RRKM calculations for the reaction rate constant.

II. Computational Details

The geometries of various intermediates and transition states were fully optimized at the unrestricted Hartree−Fock (UHF)

[⊗] Abstract published in *Advance ACS Abstracts,* May 1, 1996.

S0022-3654(95)03566-0 CCC: $12.00

level of theory using the 6-31G* basis set.[41] The calculated structures were characterized as either local minimum structures (no imaginary frequency) or transition states (one imaginary frequency) by analytical evaluation of the second derivatives of the energy at the UHF/6-31G* level. Effects of electron correlation were taken into account by further geometry optimization at the UHF MP2 (UMP2) level using the 6-31G* basis set.

Improved energy parameters were calculated at the UMP2/6-31G* structures by fourth order Moller−Plesset perturbation theory with single, double, and quadruple excitations (MP4SDQ) using the 6-31G* and 6-311G*[42] basis sets. Zero point vibrational energy corrections were taken into account by using the UHF/6-31G* frequencies scaled by 0.89. All the Moller−Plesset perturbation calculations used frozen core approximation.

For the most important intermediates and transition states, we performed single point energy calculations using the modified Gaussian-2 method,[43] G2M(rcc,MP2), proposed by us.[44] The G2M(rcc,MP2) scheme includes a series of calculations to approximate a RCCSD(T)/6-311+G(3df,2p) calculation with an additional empirical "higher level correction" based on the number of paired and unpaired electrons. The total energy is calculated as

$$E[\text{G2M(rcc,MP2)}] = E[\text{PUMP4/6-311G(d,p)}] + \Delta E(\text{RCC}) + \Delta E(+3\text{df2p}) + \Delta E(\text{HLC}) + \text{ZPE}$$

where

$$\Delta E(\text{RCC}) = E[\text{RCCSD(T)/6-31G(d,p)}] - E[\text{PUMP4/6-31G(d,p)}]$$

$$\Delta E(+3\text{df2p}) = E[\text{UMP2/6-311+G(3df,2p)}] - E[\text{UMP2/6-311G(d,p)}]$$

$$\Delta E(\text{HLC}) = -4.93n_\beta - 0.19n_\alpha, \text{ in millihartrees}$$

The G2M(rcc,MP2) method exhibits an average absolute deviation of calculated atomization energies for 32 first-row compounds of 1.28 kcal/mol. The preference of the G2M methods over original G2 is expected to be significant for the open shell systems with large spin contamination because of the use of the restricted open shell coupled cluster approach, RCCSD(T).[45]

For the G2M(rcc,MP2) scheme, the most time consuming calculation appeared to be PUMP4(SDTQ)/6-311G(d,p). To avoid it, we propose a simplified method, G2M(rcc,MP2*), which involves only UMP2 and RCCSD(T) calculations. The total energy is computed as

$$E[\text{G2M(rcc,MP2*)}] = E[\text{RCCSD(T)/6-31G(d,p)}] + E[\text{UMP2/6-311+G(3df,2p)}] - E[\text{UMP2/6-31G(d,p)}] + \Delta E(\text{HLC}) + \text{ZPE}$$

where ΔE(HLC) is exactly the same as shown for G2M(rcc,MP2). Whereas the G2M(rcc,MP2*) approach still needs to be calibrated and tested, the G2M(rcc,MP2*) results for the phenoxy radical decomposition reaction will be shown to be close to the G2M(rcc,MP2) results.

Previous theoretical studies have shown that electron correlation is important for the accurate description of the structural features of the ground state phenoxy radical.[46−49] Therefore, the UHF method may be inadequate, and we also carried out CASSCF geometry optimization of the structure and compared the results with those of UHF and UMP2. For comparison, the geometries of some intermediates and transition states have also been optimized using the hybrid density functional B3LYP approach which combines Becke's three-parameter nonlocal exchange functional[49] with the nonlocal correlation functional of Lee *et al.*[50]

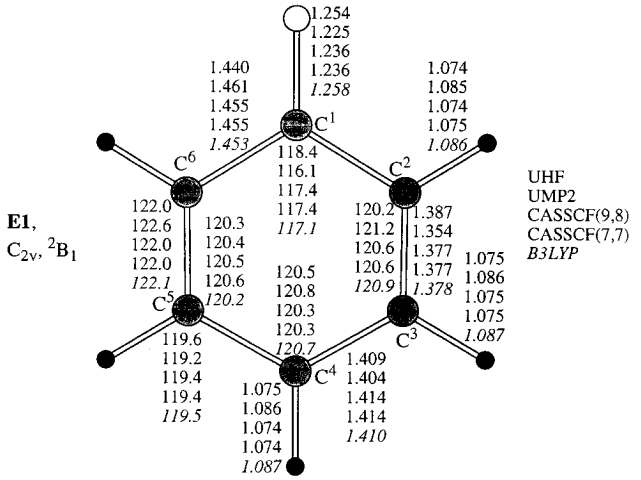

Figure 1. Comparison of structural parameters of the ground ($^2B_1$) state phenoxy radical calculated by various methods using the 6-31G* basis set. Bond distances are given in angstroms and angles in degrees.

The UHF, B3LYP, UMP2, and UMP4 calculations have been carried out using the Gaussian 92/DFT program,[51] and the CASSCF and RCCSD(T) calculations have been carried out using the MOLPRO 92 and 94 programs.[52]

III. Results and Discussion

1. Ground and Low-Lying Electronic States of the Phenoxy Radical. Molecular structure, electron spin density distribution, and vibrational frequencies of the ground state of the phenoxy radical were studied earlier by various theoretical methods and discussed in the literature.[46−49,54,55] We performed additionally the CASSCF calculations where the π active space was augmented with the lone pair orbital of the oxygen, because we were also interested in the energy separations of the low-lying electronic states. The CASSCF wave function was of (9e/8o) type, a linear combination of all the configurations resulting from distributing 9 (7 π plus 2 lone pair) electrons in 8 active orbitals. The results of these calculations were compared in Figure 1 with the literature data obtained by the UHF, UMP2, CASSCF(7e/7o), and B3LYP methods with the same 6-31G* basis set. Inclusion of the lone pair orbital into the active space had no effect on the optimized structure, and the CASSCF structural features were in agreement with the UMP2 and B3LYP results. The B3LYP/6-31G* optimized geometry and vibrational frequencies of the phenoxy radical calculated by us coincide with the data reported earlier by Qin and Wheeler.[55]

Depending on the symmetry of the singly occupied molecular orbital, the phenoxy radical has several low-lying electronic states. To obtain an idea of the ordering of the electronic states, we carried out state-specific and state-averaged CASSCF(9e/8o)/6-31G* energy calculations at the CASSCF(9e/8o)/6-31G* ground state geometry. A total of six non-totally symmetric states ($1-2\ ^2B_1$, $1-2\ ^2A_1$, and $1-2\ ^2A_2$) were included in the state-averaged calculations with equal weight. The calculated vertical excitation energies are 30.2 (33.1) kcal/mol for the 1^2B_2 state, 59.3 (62.4) kcal/mol for the 1^2A_2 state, 79.2 (77.6) kcal/mol for the 1^2B_1 state, 117.0 (120.0) kcal/mol for the 2^2B_2 state, and 139.7 (144.7) kcal/mol for the 2^2A_2 state. The numbers in front of the parentheses are the results of state-specific CASSCF, and the numbers in parentheses are the results of state-averaged CASSCF calculations. State-specific and state-averaged CASS-

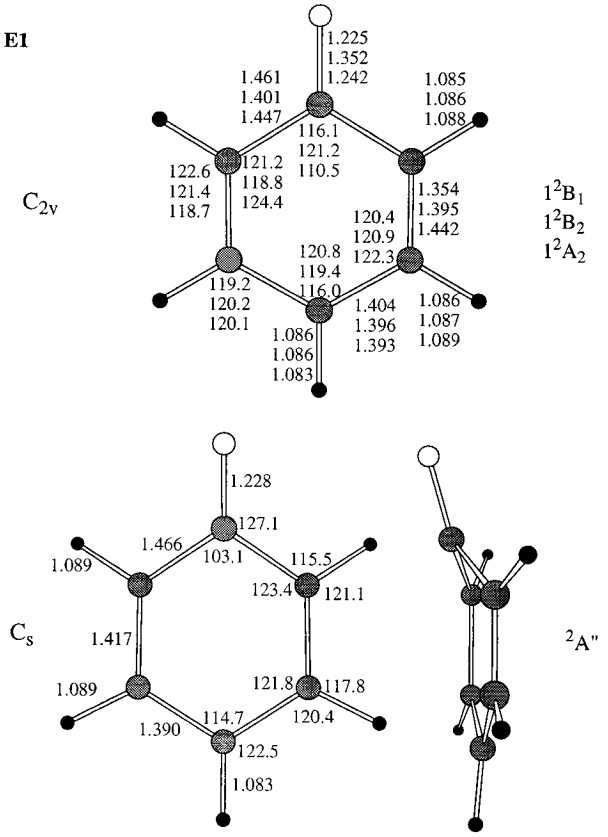

Figure 2. Comparison of the structural parameters of the lowest excited states of the phenoxy radical calculated at the UMP2/6-31G* level.

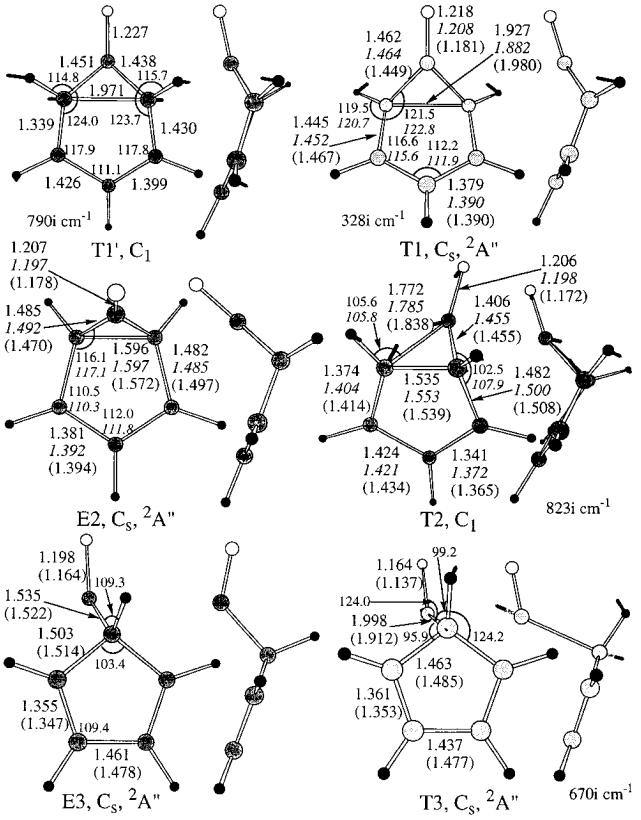

Figure 3. Structural features of the equilibrium and transition state structures along the thermal decomposition pathway by mechanism I of the phenoxy radical calculated at the UMP2 (plain numbers), B3LYP (italics), and CASSCF (in parentheses, from ref 40) levels with the 6-31G* basis set.

CF calculations produce qualitatively the same energy ordering. The difference is that the state average calculations predict slightly larger (3−5 kcal/mol) excitation energies. We just want to make a comment in passing that previous theoretical caluclations[16] on excited states have been performed with semiempirical methods, except for the 1^2A_2 state. For this state, the CIS/3-21G calculation gives an excitation energy 3 eV larger than that obtained with the CASSCF calculation with the same basis set and is totally unreliable.[16]

Several electronic excitations have been identified experimentally. From the ultraviolet photoelectron spectroscopy study of the phenide, Lineberger *et al.*[56] concluded that the first excited state of the phenoxy radical appears 24.4 ± 1.2 kcal/mol (1200 nm) above the ground state. The early experimental work of Porter *et al.*[10] on the gas phase absorption spectrum showed a band with λ_{max} at 395 nm (71.5 kcal/mol) and another band with λ_{max} at 292 nm (96.8 kcal/mol). A later experimental study[11] in a nitrogen matrix observed another band with λ_{max} at 240 nm (119.9 kcal/mol) in addition to the aforementioned spectral features, and a subsequent study of Ward[12] observed a weak and broad band at 611 nm (46.1 kcal/mol). When the calculated energies and the observed electronic transitions are compared, a reasonable assignment of the observed transitions seems to be 1200 nm to the 1^2B_2 state, 611 nm to the 1^2A_2 state, 395 nm to the 2^2B_1 state, 292 nm to the 2^2B_2 state, and 240 nm to the 2^2A_2 state. These assignments are summarized in Table 1. The most important point is that all of the calculated energies are higher than the observed transitions. As can be seen from Table 1, for the lower excited states (1^2B_1, 1^2B_2, and 1^2A_2), the calculated vertical excitation energies are about 10 kcal/mol higher than the experimental results. For the higher excited states (2^2B_2 and 2^2A_2), the calculated vertical excitation energies are about 20 kcal/mol higher than the experimental results. The discrepancy can be partly attributed to the fact that rather compact basis functions were used in our calculation while the higher excited states require more diffuse functions for an accurate description. A more essential source of the discrepancy may be the incomplete recovery of electron correlation. Dynamic electron correlation is necessary for the accurate description of the excited states. The most straightforward way to recover dynamic correlation is to perform SDCI on top of the CASSCF wave function or to carry out a CASPT2 calculation. However, for a molecule of this size, such a calculation is prohibitively expensive. Another problem with this assignment is that the $^2B_1 \rightarrow {}^2B_2$ transition is symmetry forbidden under C_{2v} symmetry, which may cast some doubt on the assignment of the 292 nm absorption to it. On the other hand, this absorption was observed[13] to be weak, and the peak due to it is almost obscured by the strong peak centered at 240 nm.

The planar UMP2/6-31G* structures of the $^2B_1$, 1^2A_2, and 1^2B_2 states of the phenoxy radical are presented in Figure 2. At the UHF/6-31G* level, these structures have no imaginary frequencies. In the ground state, the CO distance is the shortest, which is close to that of a typical CO double bond. In the 1^2B_2 state, the CO distance is noticeably longer and close to that of a typical CO single bond. The C_2C_3 distances also vary, ranging from 1.354 Å in the ground state to 1.442 Å in the 1^2A_2 state. In the $^2B_1$ and 1^2A_2 states, the CCC bond angles deviate from 120°, the CCC bond angle of benzene. The large variations in the CC bond distances and CCC bond angles of the $^2B_1$ and 1^2A_2 states of the phenoxy radical indicate that the aromaticity of the benzene ring is not preserved in the π states of the phenoxy radical. On the other hand, all the CC bond distances of the 1^2B_2 state are close to 1.4 Å, and all the CCC bond angles are close to 120°, indicating that the aromaticity of the benzene ring is largely intact in the 1^2B_2 state of the phenoxy radical.

TABLE 1: Calculated[a] and Experimental Vertical Excitation Energies[b] of the Phenoxy Radical

state	1^2B_1	2^2B_1	1^2B_2	2^2B_2	1^2A_2	2^2A_2
sa-CASSCF[c]	−304.97774	77.6 (0.341)	33 (0.0)	120.0 (0.0)	62.4 (0.128)	144.7 (0.691)
ss-CASSCF[d]	−304.98703	79.2	30.2	117.0	59.3	139.7
exptl		71.5[e]	24.4[f]	96.8[e]	46.1[g]	119.9[h]

[a] The calculations used the 6-31G* basis set and were carried out at the CASSCF(9e/8o) geometry of the ground state. [b] The energy of the ground state is given in hartrees, the energies of the other states are given relative to the ground state in kilocalories/mole. [c] Results of state-averaged CASSCF(9e/8o) calculations in which the six electronic states shown in this table are included with equal weight. The numbers in parentheses are calculated transition moments from the ground state. [d] Results of state-specific CASSCF(9e/8o) calculations. [e] Reference 10. [f] Reference 56. [g] Reference 12. [h] Reference 11.

TABLE 2: Energies of the Low-Lying Electronic States of the Phenoxy Radical and Critical Structures along the Thermal Decomposition Pathway by Mechanism I[a]

method	E1 ($^2B_1$)[b]	E1 ($^2B_2$)	E1 ($^2A_2$)	E1 ($^2A''$)	T1′	T1	E2	T2	E3	T3	$C_5H_5 + CO$
$\langle S^2\rangle$[c]	1.30	1.22 (1.22)[d]	0.84 (0.85)[d]	0.83	1.08	0.92	0.95	1.15	0.76	0.89	0.96
ZPE[e]	53.6	54.2	54.3	55.0	51.9	53.3	53.1	51.9	52.2	50.8	49.6
UMP2											
6-31G*	0.82315	20.3 (31.9)[d]	33.6 (44.8)[d]	29.8	42.4	35.2	29.6	44.9	10.3	16.3	7.5
6-31G**	0.86220					42.3	35.0	29.4	44.7	10.1	
6-311G*	0.93505	20.1 (29.6)[d]	33.2 (44.6)[d]		41.4	34.1	28.8	42.9	6.5	16.4	3.8
6-311G**	0.97062				41.2	33.7		42.5			
6-311+G(3df,2p)	1.15866				40.0	33.4	29.0	42.2	9.8		
PUMP2[f]											
6-31G*	0.85326	25.9 (37.4)[d]	48.6 (59.6)[d]		50.3	46.5	39.8	51.1	27.9	32.9	26.4
6-311G*	0.96492	26.0 (35.6)[d]	47.9 (59.0)[d]		49.5	45.4	39.0	48.4	25.2	28.9	14.5
PUMP3[f]											
6-31G*	0.88879	24.2 (36.8)[d]	56.2 (67.0)[d]		57.6	55.4	46.8	60.5	35.9	41.4	22.8
6-311G*	0.99747	24.3 (35.1)[d]	52.9 (67.0)[d]		57.6	55.3	46.6	59.7	34.4	38.7	20.1
UMP4SDQ											
6-31G*	0.88286	21.5 (33.7)[d]	45.3 (56.1)[d]		50.0	45.9	37.8	53.7	22.0	29.2	11.4
6-311G*	0.99223	21.9 (32.2)[d]	45.4 (56.4)[d]		49.6	45.5	37.2	52.3	20.3	26.2	8.2
PUMP4[f]											
6-31G**	0.98101				51.5	48.7	42.3	53.0	29.7		
6-311G**	1.09310				50.1	47.0		50.4			
RCCSD(T)											
6-31G**	0.97675				52.0	50.9	44.1	54.7	30.4		
B3LYP/6-31G*	1.82769					51.7	48.6	56.6			
CASPT2/6-31G**[g]	0.93758				51.0	44.1	53.9	28.8	33.6		
G2M(rcc,MP2)	1.342883				49.5	48.9		51.9			
G2M(rcc,MP2*)	1.273214				49.7	49.3	43.7	52.2	30.0		
exptl			(24.4)[h]	(46)[i]					44[j]		

[a] Calculated at UMP2/6-31G* geometries, energies are given in kilocalories/mole relative to E1 ($^2B_1$). Zero-point energy corrections are included. [b] Total energies, $-305 - E_{tot}$, in hartrees. [c] Expectation values of the total spin operator, $S(S + 1)$, of the UHF wave function. [d] Numbers in parentheses are calculated at the UMP2/6-31G* geometry of the $^2B_1$ state. [e] Zero-point energies calculated at the UHF/6-31G* level and scaled by 0.89. [f] PUMP2, PUMP3, and PUMP4 are spin-projected UMP2, UMP3, and UMP4(SDTQ) energies, respectively. After projection, the expection value of S^2 is 0.75 for all structures. [g] From ref 40. [h] From the photoelectron spectrum of the phenolate anion, a weak and broad band at about 1 eV higher than the signal of the ground state phenoxy radical was detected and attributed to the $^2B_2$ state of the radical, ref 56. [i] A weak and broad absorption at 611 nm was detected in the electronic spectrum of the phenoxy radical in aqueous solution and was attributed to the $^2B_1 \rightarrow {}^2A_2$ excitation, ref 16. [j] Activation energy of thermal decomposition of the phenoxy radical obtained from kinetic studies, refs 5 and 37.

2. Mechanism for the Thermal Decomposition of C_6H_5O ($^2B_1$). Geometries of the transition states and intermediates for the thermal decomposition mechanism I of the phenoxy radical are presented in Figure 3. These structures were obtained from geometry optimization at the UMP2/6-31G* level starting from the corresponding UHF/6-31G* structures and Hessian. The arrows and the numbers in cm^{-1} in Figure 3 indicate the imaginary vibrational mode vector and frequency, respectively, obtained from the UHF/6-31G* vibrational analysis. Structures T1, E2, and E3 have C_s symmetry, structures T1′, T2, and T3 none. The total energies of the structures at different levels of theory are presented in Table 2.

In the first step of the decomposition process, E1 ($^2B_1$) isomerizes to E2 ($^2A''$). Singly occupied molecular orbitals of E1 ($^2B_1$) and E2 ($^2A''$) are shown in Figure 4. The $^2B_1$ electronic state of the phenoxy radical does not correlate with that of E2, and the E1 ($^2B_1$) → E2 ($^2A''$) isomerization is a symmetry-forbidden process. Instead, E2 correlates with the $^2A_2$ electronic state of E1, the lowest excited π state of the phenoxy radical. Thus, if the thermal decomposition proceeds via the intermediate E2 with C_s symmetry, there must be a change in the electronic state from $^2B_1$ ($^2A'$ in terms of C_s symmetry) to $^2A''$. Therefore, we looked for the lowest point on the seam of crossing between $^2A'$ and $^2A''$ surfaces within C_s symmetry where the mirror plane of symmetry contains two carbons, one oxygen, and one hydrogen and reflects four carbons and four hydrogens. For the search, we used an improved version of the algorithm implemented in the HONDO 8.4 program.[57] The geometry of the lowest point X1 on the ($^2A'$,$^2A''$) seam of crossing optimized at the UMP2/6-31G* level is shown in Figure 5. At this level of theory, the energy of X1 is 29.2 kcal/mol relative to the ground state of the phenoxy radical.

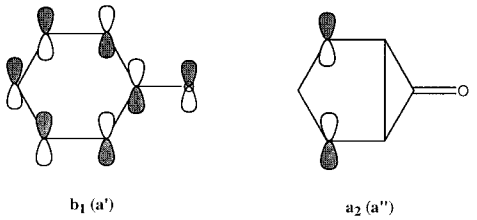

Figure 4. Schematic singly occupied molecular orbitals for the ground state phenoxy radical and the intermediate E2.

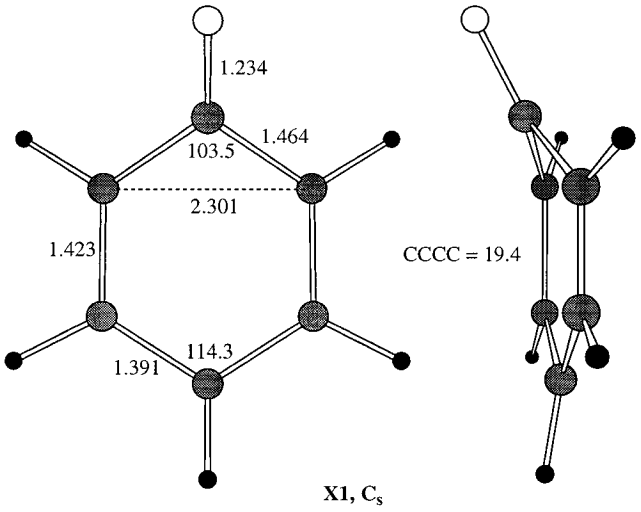

Figure 5. Structural features and energy of the minimum on the seam of crossing between the ^{2}A′ and ^{2}A″ surfaces of the phenoxy radical calculated at the UMP2/6-31G* level.

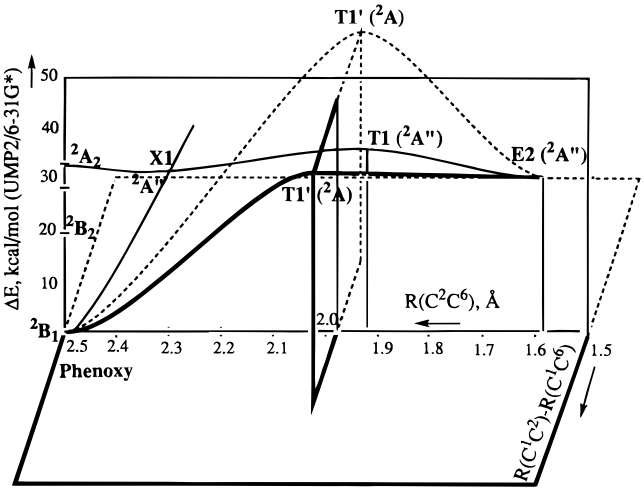

Figure 6. Profile of the potential energy surface for the E1 (^{2}B$_1$) → E2 (^{2}A″) isomerization calculated at the UMP2/6-31G* level.

The transition state T1 possesses C_s symmetry and a ^{2}A″ electronic state, the same as for E2. The UMP2/6-31G* + ZPE energy of T1 is 35.2 kcal/mol with respect to E1 (^{2}B$_1$). Thus, T1 lies on the ^{2}A″ surface and higher than X1. Comparison of the geometries for X1 and T1, particularly of the C_2C_6 distances, showed that the (^{2}A′,^{2}A″) crossing occurs before the transition state T1. As illustrated in Figure 6, if the rearrangement takes place within C_s symmetry, the system travels along the ^{2}A′ surface, switches to the ^{2}A″ surface at X1, overcomes the barrier at T1, and reaches the intermediate E2.

Meanwhile, the E1 (^{2}B$_1$) → E2 (^{2}A″) isomerization can take place by the breaking of symmetry. The nonsymmetric transition state T1′ lies 42.4 kcal/mol higher than the ground state of the phenoxy radical at the UMP2/6-31G* level with ZPE. As seen in Figure 6, two optically different conformations of T1′ must exist. The geometries of T1 and T1′ are alike, but T1′ has a longer C_2C_6 distance, 1.97 Å vs 1.93 Å in T1. The CC bond lengths in T1′ are close to those in E1 (^{2}B$_1$), except for the shortened C_5C_6 distance. On the contrary, in T1 the CC bond lengths are similar to those in E1 (^{2}A$_2$). To confirm the connections of T1 and T1′, we performed intrinsic reaction coordinate (IRC) calculations starting from these transition states using the algorithm of Schlegel and Gonzalez[58] implemented in Gaussian 92. The calculations show T1′ to be connected to E1 (^{2}B$_1$) on the reactant side and to E2 on the product side. For T1, the forward IRC calculations converge to E2, while the reverse calculations lead to the nonplanar excited isomer of the phenoxy radical, E1 (^{2}A″). The geometry of the latter is drawn in Figure 2. The energy of E1 (^{2}A″), 28.4 kcal/mol at the UMP2/6-31G* level, is lower than that of E1 (^{2}A$_2$). At this level of theory, the E1 (^{2}A$_2$) structure having C_{2v} symmetry is not a local minimum and the lowest excited π electronic state of the phenoxy radical has a nonplanar equilibrium structure. However, this result is most likely an artifact of the UMP2 method. At the CASSCF(7e/7o) level[16] the ^{2}A$_2$ structure within C_{2v} symmetry has no imaginary frequencies and is a local minimum. The geometries and energies of E1 (^{2}A″) and X1 are almost identical; the (^{2}A′,^{2}A″) crossing occurs in the close vicinity of E1 (^{2}A″). The difference in the imaginary frequency values, 790i cm^{-1} in T1′ vs 328i cm^{-1} in T1, is attributed to the difference in the corresponding reaction heats. T1′ connects E1 (^{2}B$_1$) with E2, the reaction has a high endothermicity, and the barrier is narrow. T1 connects E1 (^{2}A″) and E2, the reaction is nearly thermoneutral, and the barrier is much broader.

At the UMP2/6-31G* + ZPE level, T1′ is 7.2 kcal/mol higher in energy than T1. However, when the theory level rises, the energies of T1′ and T1 come closer. At our best level, G2M-(rcc,MP2), T1′ lies 0.6 kcal/mol higher than T1. If both T1 and T1′ transition states exist on the potential energy surface, they must be separated by a second order top. Geometries of T1 and T1′ are similar, and the energies are also close at high theory levels. This indicates that the two transition states may merge in one TS and the second order top between them may disappear at the higher level potential energy surfaces. This hypothesis is supported by the B3LYP optimization of T1 and T1′; starting with T1′ UMP2 geometry, it converges to T1. At the CASSCF/3-21G level, Olivella *et al.*[40] have found an asymmetric TS (T1′), but at the higher CASSCF/6-31G(d) level the optimization converges to a symmetric TS (T1). Thus, the existence of the nonsymmetric transition state T1′ at the UMP2/6-31G* level is apparently an artifact of this approximation.

From the intermediate E2, the reaction proceeds by the α-CC bond cleavage leading to the formation of the five-membered ring C_5H_5CO intermediate E3. Like E2, E3 has C_s symmetry and ^{2}A″ electronic state but the symmetry plane moves. Therefore, the transition state T2 between E2 and E3 has no symmetry. The E2 → T2 → E3 step has the highest barrier on the potential energy surface for this decomposition mechanism. Finally, E3 eliminates the CO group to form the main reaction products, cyclopentadiene radical, C_5H_5, and carbon monoxide. Transition state T3 corresponds to the dissociation of CO and the barrier is low, 4−7 kcal/mol relative to E3 at various levels of theory.

As seen in Figure 3, the UMP2, B3LYP, and CASSCF optimized geometries are in general agreement. The UMP2 energies are strongly affected by spin contamination. The expectation value, $\langle S^2 \rangle$, of a pure doublet state is 0.75. As can be seen in Table 2, at the UHF/6-31G* level, all the expectation values are significantly larger than that of a pure doublet state. The ^{2}B$_1$ and ^{2}B$_2$ states are most severely affected. Therefore, the removal of the spin contamination is expected to lower the energy of these two states more than the other states. It results in a larger energy gap between the ground state structure and the other structures in Table 2. This argument is in agreement with the PUMP2 results (Table 2). After spin projection, all the $\langle S^2 \rangle$ values are 0.75. Second, the UMP4SDQ results are in better agreement with the results of PUMP2 than with those of

TABLE 3: Moments of Inertia and Vibrational Frequencies of Various Intermediates and Transition States Calculated at the B3LYP/6-31G* Level

species or transition state	*i*	I_i (10^{-4} g cm^2)	ν_j (cm^{-1})
E1	A	153.5	195, 378, 444, 486, 531, 599, 657, 795, 805, 811,
	B	304.4	921, 972, 986, 993, 1018, 1099, 1176, 1178, 1289, 1353,
	C	457.9	1434, 1459, 1499, 1565, 1604, 3188, 3194, 3210, 3221, 3223
T1	A	136.8	370i, 214, 302, 433, 512, 589, 620, 703, 733, 776,
	B	337.5	870, 894, 908, 979, 985, 1073, 1084, 1113, 1139, 1263,
	C	423.3	1311, 1360, 1443, 1510, 1869, 3146, 3148, 3213, 3218, 3239
E2	A	145.9	139, 225, 459, 468, 563, 607, 653, 706, 733, 796,
	B	332.2	890, 913, 928, 965, 1011, 1021, 1066, 1085, 1120, 1238,
	C	389.4	1266, 1325, 1416, 1477, 1936, 3142, 3149, 3220, 3246, 3254
T2	A	135.9	624i, 153, 283, 412, 431, 553, 723, 747, 769, 788,
	B	352.1	829, 894, 946, 984, 1011, 1079, 1088, 1096, 1140, 1250,
	C	414.1	1304, 1387, 1439, 1543, 1895, 3037, 3223, 3234, 3248, 3255

UMP2, indicating that the problem of spin contamination is remedied by higher order perturbation correction and higher order excitations. Third, at all the levels of theory applied, the highest energy barrier for thermal decomposition of the phenoxy radical is at structure T2. Previous experimental kinetic studies[37,39] derived an activation energy of 44 kcal/mol for the thermal decomposition of the phenoxy radical. When the calculated energy difference between T2 and the ground state phenoxy radical is compared, it seems that the UMP2 results are in best agreement with the activation energy obtained from kinetic studies. This is, however, fortuitous and due to different degrees of spin contamination in the wave functions of the two structures. The PUMP2 and UMP4SDQ energies of T2 are about 10 kcal/mol higher than the experimental result. Higher level PUMP4(SDTQ), RCCST(T), and G2M(rcc,MP2) calculations confirm the UMP4SDQ values. The energies seem to converge as with the correlation treatment using the same basis set. The results do not change much in going from the UMP4SDQ level to PUMP4(SDTQ) and RCCSD(T) and from the 6-31G** basis set to 6-311G** and 6-311+G(3df,2p). Multireference CASPT2 energies[40] are almost identical to the RCCSD(T) values. Hence, we expect the calculated G2M-(rcc,MP2) relative energies for the transition states T1, T1′, and T2 to be reliable. G2M* energies for these structures agree well with the G2M(rcc,MP2) energies with deviations of only 0.2−0.4 kcal/mol.

The least computationally intensive B3LYP method performs well. The B3LYP/6-31G* relative energies for T1, E2, and T2 are overestimated by 1−4 kcal/mol in comparison to those calculated at the RCCSD(T) and CASPT2 levels of theory. The B3LYP energetics for this reaction is more accurate than the UMP2 one.

Mechanism II is not considered here. At the CASPT2//CASSCF level,[40] transition state T4 lies 18.4 kcal/mol higher than T1. The rate-controlling step for mechanism II is the cyclization of E4 via transition state T5. Olivella *et al.*[40] found T5 to lie 20.1 kcal/mol higher than T2, the critical transition state for mechanism I. Hence, mechanism II is not expected to compete with I.

3. RRKM Calculations of the Rate Constant for CO Production. The rate constant for CO formation has been calculated with the RRKM theory[59] according to the following mechanism:

$$\mathrm{E1} \underset{-\mathrm{a\ (+M)}}{\overset{\mathrm{a\ (+M)}}{\rightleftharpoons}} \mathrm{E1}^{\dagger} \underset{-\mathrm{b}}{\overset{\mathrm{b}}{\rightleftharpoons}} \mathrm{E2}^{\dagger} \overset{\mathrm{c}}{\rightarrow} \mathrm{CO} + \mathrm{C_5H_5}$$

Where "†" stands for vibrational excitation and k_a[M] and k_{-a}[M] represent collisional activation and deactivation, respectively. Steady-state analysis for the vibrationally excited species gives rise to the following expression for the first-order rate coefficient of CO formation:

$$k = \frac{l_b^{\ddagger} Q_{rb}^{\ddagger}}{h Q_1} e^{-E^{\circ}_b/RT} \int_0^{\infty} \frac{\omega G(E)\, N_b(E_b^{\ddagger}) e^{-E_b^{\ddagger}/RT}\, dE_b^{\ddagger}}{\omega + k_b(E) - F(E)} \qquad \text{(I)}$$

where

$$G(\mathrm{E}) = k_c(\mathrm{E})/[k_{-b}(\mathrm{E}) + k_c(\mathrm{E})] \qquad \text{(II)}$$

$$F(\mathrm{E}) = k_b(\mathrm{E}) k_{-b}(\mathrm{E})/[k_{-b}(\mathrm{E}) + k_c(\mathrm{E})] \qquad \text{(III)}$$

and

$$k_i(E) = l_i^{\ddagger} I_i N_i(E_i^{\ddagger})/h\rho(E) \qquad \text{(IV)}$$

In eq I, E°_b is the reaction barrier for step b, forming the bicyclointermediate, E2. ω is the effective collision frequency, k_{-a}[M] = $\beta_c Z_{LJ}$[M], evaluated with Troe's weak collision approximation[60] using experimentally measured Lennard-Jones parameters for chlorobenzene[61] and Ar[62] to calculate the collision frequency Z_{LJ}[M]. Q_1 is the rovibrational partition function of E1, $Q_{v1}Q_{r1}$, and $Q_{rb}^{\ddagger}$ is the rotational partition of the transition state in step b, T1. $E_b^{\ddagger}$ is the excess energy above T1 and $l_b^{\ddagger}$ is the reaction path degeneracy or statistical factor for step b, which is 2 for the E1 → E2 isomerization process. The lower limit for the integration in eq I should be the difference in energies between T2 and T1, 2.9 kcal/mol, but is ∼0 because $k_c(E)$ or $G(E)$ is zero at E ≤ E° = 52.2 kcal/mol.

Equation II gives the probability for CO production from E2, and eq III represents the specific rate constant for E2 returning to E1. The specific rate constant given in eq IV, originally derived by Marcus,[59] provides the probability for the isomerization and/or decomposition of the excited E1 and E2. In this equation, $l_i^{\ddagger}$ is the statistical factor for reaction step *i* as defined above; $N_i(E_i^{\ddagger})$ is the sum of states of the TS associated with step *i* with excess energy $E_i^{\ddagger} = E - E^{\circ}$. $\rho(E)$ is the density of states of either E1 or E2 at total energy E; I_i is the ratio of the overall rotational partition functions of the transition state and the reactant in step *i*.

Other quantities given in the above equations have their customary meanings. Equation I was evaluated using the G2M* energetics and B3LYP molecular parameters given in Table 3 and the procedure employed in an earlier treatment for reversible isomerization reactions by Lin and Laidler.[63]

Figure 7 represents the computed specific constants for steps b, −b, and c; the result indicates that $k_{-b}(E) > k_c(E) \gg k_b(E)$ throughout the range of energy of interest because of the small barriers for the isomerization (via −b) and decomposition (via c) of E_2. Figure 8 compares the calculated and extrapolated experimental first-order rate constant (k^{∞}) for the production of

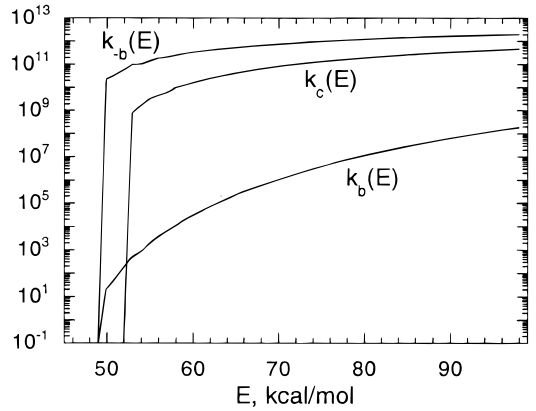

Figure 7. Calculated rate constants for steps b, −b, and c as a function of energy.

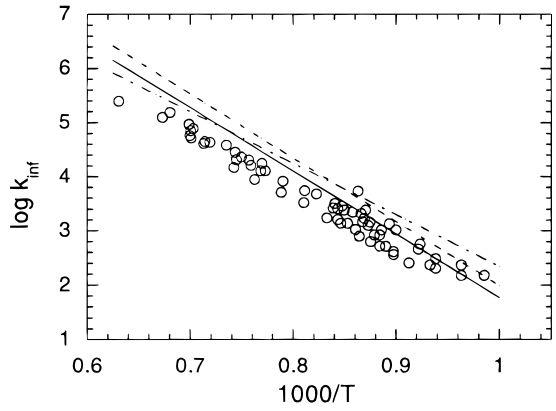

Figure 8. Arrhenius plot for the calculated and extrapolated experimental first-order rate constant (k^{∞}) for the production of CO. The experimental results from ref 5 obtained at $P = 0.5-0.9$ atm, converted to the high-pressure limit by means of the relationship $k_{\infty} = k_{exp}/(k_p/k_{\infty})_{th}$, where the fall-off ratio (k_p/k_{∞}) is the theoretical rate constant ratio calculated with eq I at $P = P_{exp}$ and $P = \infty$, are shown by open circles. Solid and dashed lines are theoretical rates calculated from eqs I and V, respectively. The dashed-and-dotted line corresponds to the experimental rate reported in ref 6.

CO. The experimental results of Lin and Lin[5] obtained at $P = 0.5-0.9$ atm have been converted to the high-pressure limit by means of the relationship $k_{\infty} = k_{exp}/(k_p/k_{\infty})_{th}$, where the fall-off ratio $(k_p/k_{\infty})_{th}$ is the theoretical rate constant ratio calculated with eq I at $P = P_{exp}$ and $P = \infty$.

The theoretical and experimental values agree closely at $T < 1200$ K, above which they deviate from each other. In Figure 8, we compare the theoretically predicted rate constant using the conventional single transition state RRKM formulation assuming step c to be the rate-limiting process. Equation I contracts to the well-known expression for a single barrier decomposition process:

$$k = \frac{I_c^{\ddagger} Q_{rc}^{\ddagger}}{hQ_1} e^{-E_c^{\ddagger}/RT} \int_0^{\infty} \frac{\omega N_c(E_c^{\ddagger}) e^{-E_c^{\ddagger}/RT}\, dE_c^{\ddagger}}{\omega + k_c(E)}$$

if one sets $k_b(E) = k_c(E)$ and $k_{-b}(E) = 0$. Equation V gives a higher value of the first-order rate constant for CO production.

Figure 9 shows the effect of pressure on the unimolecular rate constant at 1000 and 1586 K. At both temperatures, eq V predicts a slightly faster fall-off in k/k_{∞} than that calculated by eq I which contains terms for the reversible reaction, E2 → E1. Because the effect of pressure results from the relative magnitude of ω vs $[k_b(E) - F(E)]$ in eq I and ω vs $k_c(E)$ in eq V, the influence of the reverse reaction manifested by the $F(E)$ term in the former is clear and reasonable.

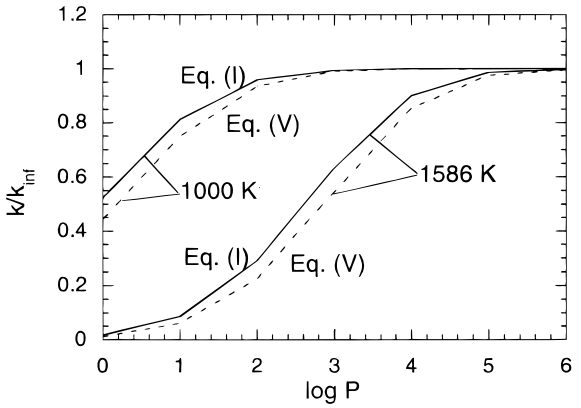

Figure 9. Unimolecular rate constants as a function of pressure. Solid and dashed lines show the rate calculated on the basis of eqs I and V, respectively.

TABLE 4: Relative Energies (kcal/mol)[a] of the Critical Structures along Mechanisms II and III

method	E1	T4	E4	T5	T6	$C_2H_2HCCO + C_2H_2$	$HCCO + 2C_2H_2$
CASPT2/6-31G(d,p)[b]	0.0	69.6	69.4	74.0			
B3LYP/6-31G(d)	0.0			78.5	117.7	96.3	110.5

[a] Relative to C_6H_5O (E1). ZPE corrections are included. [b] From ref 40.

Although the agreement between theory and experiment is fair, the deviation at higher temperatures ($T > 1200$ K) has to be addressed. The deviation might be a result of the "draining" of C_6H_5O by other non-CO producing channels at $T > 1200$ K, such as sequential scission of three CC bonds, C_6H_5O → OC═CHCH═CHCH═CH (E4) → T6 → OC═CHCH═CH + C_2H_2 → OC═CH + $2C_2H_2$, or concerted scission of these bonds, C_6H_5O → OC═CH + $2C_2H_2$. The ketenyl radical produced in these processes is too stable to produce CO directly. The sequential mechanism is designated as III in Scheme 1. The transition state for the rupture of the α-CC bond is T4 and the barrier is 69.6 kcal/mol at the CASPT2 level[40] (Table 4). We calculated transition state T6 for the cleavage of the second CC bond at the B3LYP level. For comparison, we also recalculated transition state T5, which is critical for mechanism II, at this level of theory. Optimized geometries are shown in Figure 10. CASSCF and B3LYP approximations give very close geometric parameters for T5. The B3LYP relative energy of T5 at the B3LYP level deviates from the more reliable CASPT2 value by only 4.5 kcal/mol. The B3LYP energy of T6, connecting E4 to OC═CHCH═CH + C_2H_2, is calculated as 117.7 kcal/mol, much higher than the energy of T5. This is not surprising because the CC bond scission is a highly endothermic process; OC═CHCH═CH + C_2H_2 lie 96.3 kcal/mol higher than the phenoxy radical at the B3LYP level. The reverse barrier is 21.4 kcal/mol. Hence, mechanism III cannot compete effectively with mechanisms II and I and it cannot "drain" C_6H_5O. With regard to the concerted process, a search of the transition state shows that it does not exist, the optimization converges to T6. The C_6H_5O → OC═CH + $2C_2H_2$ dissociation is endothermic by 110.5 kcal/mol at the B3LYP level, and it can neither compete with mechanisms I and II nor produce CO.

IV. Conclusions

On the basis of the agreement between the calculated and experimental ordering of the vertical excitation energies of the

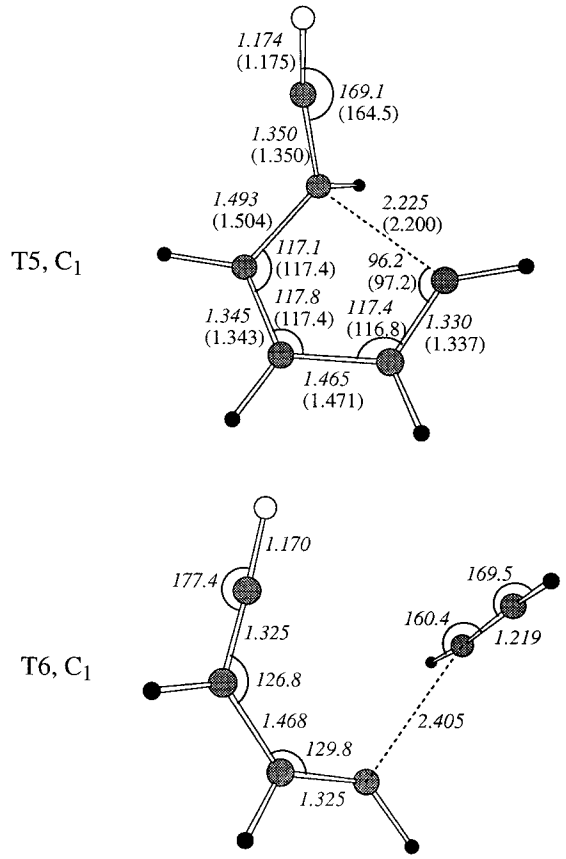

Figure 10. Geometries of transition states T5 and T6 optimized at the B3LYP/6-31G* (numbers in italics) and CASSCF/6-31G* (numbers in parentheses, from ref 40) levels of theory.

phenoxy radical, the assignment of the first electronic transition at 1200 nm to the $^2B_1 \rightarrow {}^2B_2$ excitation was confirmed. The results also suggest the reassignment of the second and third electronic transitions at 600 and 395 nm to the $^2A_2$ and 2^2B_1 excitations, respectively. The optical absorptions at 292 and 240 nm are tentatively assigned to the $^2B_1 \rightarrow 2^2B_2$ and $^2B_1 \rightarrow 2^2A_2$ transitions.

The thermal decomposition of the phenoxy radical is confirmed to proceed by mechanism I through the dual-ring intermediate E2 followed by the α-CC bond scission leading to E3 and elimination of CO, resulting in the main reaction product, $C_5H_5 + CO$. The first reaction step, the E1 ($^2B_1$) → E2 ($^2A''$) isomerization is a symmetry-forbidden process which can take place either via the nonsymmetric transition state T1′ or via the lowest point on the ($^2A'$,$^2A''$) seam of crossing X1 and TS T1 within C_s symmetry. T1′ and T1 have close energies of about 49 kcal/mol at our best theory level. E2 is stabilized by about 6 kcal/mol with respect to T1 and T1′. The next step, E2 → E3, occurs via TS T2 and is rate-controlling with the calculated barrier of 52 kcal/mol relative to the phenoxy radical. The dissociation of E3 to $C_5H_5 + CO$ has a low barrier.

RRKM calculations for the rate constant give the values close to experiment, especially for the temperatures below 1200 K. Further analysis and modeling of the experimental data are required to reconcile the deviation between the theoretical and experimental rate constants at higher temperatures.

Acknowledgment. We are obliged to the Cherry L. Emerson Center for Scientific Computations for the use of various programs and computing facilities. Part of the calculations have been performed on the supercomputer Cray C90 in the Pittsburgh Supercomputing Center within the Grant #CHE940026P. K.M. acknowledges the support received from the Air Force Office for Scientific Research through the Grant F49620-95-1-0182. M.C.L. acknowledges the support received from the Department of Energy, Office of Basic Energy Sciences, Division of Chemical Sciences through Contract DE-FGO5-91ER14191. Appreciation is also expressed to Prof. K. M. Dunn for his assistance in the searching the minimum of crossing seam.

References and Notes

(1) Longwell, J. P. In *Alternate Hydrocarbon Fules: Combustion and Chemical Kinectis*; Bowman, C. T., Birkeland, J., Eds.; American Institute of Aeronautics and Astronautics: New York, 1978; p 3.
(2) Norrish, R. G. W.; Taylor, G. W. *Proc. R. Soc. London, A* **1956**, *234*, 160.
(3) Fujii, N.; Asaba, T. *Proceedings of the 14th Symposium on Combustion*; The Combustion Institute: Pittsburgh, PA, 1973; p 433.
(4) Howard, J. A. In *Free Radicals*;; Kochi, J. K., Ed.; Wiley: New York, 1973; Vol. 2, p 3.
(5) Lin, C.-Y.; Lin, M. C. *Int. J. Chem. Kinet.* **1985**, *17*, 1025; *J. Phys. Chem.* **1986**, *90*, 425.
(6) Frank, P.; Herzler, J.; Just, Th.; Wahl, C. *Proceedings of the 25th International Symposium on Combustion*; The Combustion Institute: Pittsburgh, PA, 1994; p 833.
(7) Sibener, S. J.; Buss, R. J.; Casavecchia, P.; Hirooka, T.; Lee, Y. T. *J. Chem. Phys.* **1980**, *72*, 4341.
(8) Eriksson, L. E. G.; Hyde, J. S.; Ehrenberg, A. *Biochem. Biophys. Acta* **1969**, *192*, 211.
(9) Weaver, E. C. *Annu. Rev. Plant Physiol.* **1968**, *19*, 283.
(10) Land, E. J.; Porter, G.; Strachan. *Trans. Faraday Soc.* **1961**, *57*, 1885.
(11) Roebber, J. L. *J. Chem. Phys.* **1962**, *37*, 1974.
(12) Ward, B. *Spectrochim. Acta A* **1968**, *24*, 813.
(13) Bent, D. V.; Haydon, E. *J. Am. Chem. Soc.* **1975**, *97*, 2599.
(14) Schuler, R. H.; Buzzard, G. K. *Int. J. Radiat. Phys. Chem.* **1976**, *8*, 563.
(15) Pullin, D.; Andrews, L. *J. Mol. Struct.* **1982**, *95*, 181.
(16) Johnston, L. J.; Mathivanan, N.; Negri, F.; Siebrand, W.; Zerbetto, F. *Can. J. Chem.* **1993**, *71*, 1655.
(17) Hinchliffe, A.; Steinbank, R. E.; Ali, M. A. *Theor. Chim. Acta* **1966**, *5*, 95.
(18) Chang, H. M.; Jaffe, H. H. *Chem. Phys. Lett.* **1973**, *23*, 146.
(19) Chang, H. M.; Jaffe, H. H.; Masmandis, C. A. *J. Phys. Chem.* **1975**, *79*, 1118.
(20) Stone, T. J.; Waters, W. A. *Proc. Chem. Soc.* **1962**, 253.
(21) Dixon, W. T.; Norman, R. O. C. *Proc. Chem. Soc.* **1963**, 97.
(22) Stone, T. J.; Waters, W. A. *J. Chem. Soc.* **1964**, 213.
(23) Dixon, W. T.; Norman, R. O. C. *J. Chem. Soc.* **1964**, 4857.
(24) Neta, P.; Fessenden, R. W. *J. Phys. Chem.* **1974**, *78*, 523.
(25) Dixon, W. T.; Murphy, D. *J. Chem. Soc., Faraday Trans. 2* **1976**, *72*, 1221.
(26) Pople, J. A.; Beveridge, D. L.; Dobosh, P. A. *J. Am. Chem. Soc.* **1968**, *90*, 4201.
(27) Lloyd, R. V.; Wood, D. E. *J. Am. Chem. Soc.* **1974**, *96*, 659.
(28) Hinchliffe, A. *Chem. Phys. Lett.* **1974**, *27*, 454.
(29) Shinagawa, Y.; Shinagawa, Y. *J. Am. Chem. Soc.* **1978**, *100*, 67.
(30) Armstrong, D. R.; Cameron, C.; Nonhebel, D.; Perkins, P. G. *J. Chem. Soc., Perkin Trans.* **1983**, *2*, 569.
(31) Beck, S. M.; Brus, L. E. *J. Chem. Phys.* **1982**, *76*, 4700.
(32) Tripathi, G. N. R.; Schuler, R. H. *Chem. Phys. Lett.* **1983**, *98*, 594.
(33) Tripathi, G. N. R.; Schuler, R. H. *J. Chem. Phys.* **1984**, *81*, 113.
(34) Johnson, C. R.; Ludwig, M.; Asher, S. A. *J. Am. Chem. Soc.* **1986**, *108*, 905.
(35) Tripathi, G. N. R.; Schuler, R. H. *J. Phys. Chem.* **1988**, *92*, 5129.
(36) Tripathi, G. N. R. In *Time Resolved Spectroscopy*; Clark, R. J. H., Hester, R. E., Eds.; Wiley: New York, 1989; p 157.
(37) Colussi, A. J.; Zabel, F.; Benson, S. W. *Int. J. Chem. Kinet.* **1977**, *9*, 161.
(38) Harrison, A. G.; Honnen, L. R.; Dauben, H. J.; Lossing, F. P. *J. Am. Chem. Soc.* **1960**, *82*, 5593.
(39) Schmoltner, A.-M.; Anex, D. S.; Lee, Y. T. *J. Phys. Chem.* **1992**, *96*, 1236.
(40) Olivella, S.; Sole, A.; Garcia-Raso, A. *J. Phys. Chem.* **1995**, *99*, 10549.
(41) Hehre, W. J.; Ditchfield, R.; Pople, J. A. *J. Chem. Phys.* **56**, 2257.
(42) Krishnan, R.; Frisch, M.; Pople, J. A. *J. Chem. Phys.* **1980**, *72*, 4244.
(43) (a) Curtiss, L. A.; Raghavachari, K.; Trucks, G. W.; Pople, J. A. *J. Chem. Phys.* **1991**, *94*, 7221. (b) Pople, J. A.; Head-Gordon, M.; Fox, D.

J.; Raghavachari, K.; Curtiss, L. A. *J. Chem. Phys.* **1989**, *90*, 5622. (c) Curtiss, L. A.; Jones, C.; Trucks, G. W.; Raghavachari, K.; Pople, J. A. *J. Chem. Phys.* **1990**, *93*, 2537.

(44) Mebel, A. M.; Morokuma, K.; Lin, M. C. *J. Chem. Phys.* **1995**, *103*, 7414.

(45) (a) Purvis, G. D.; Bartlett, R. J. *J. Chem. Phys.* **1982**, *76*, 1910. (b) Hampel, C.; Peterson, K. A.; Werner, H.-J. *Chem. Phys. Lett.* **1992**, *190*, 1. (c) Knowles, P. J.; Hampel, C.; Werner, H.-J. *J. Chem. Phys.* **1994**, *99*, 5219. (d) Deegan, M. J. O.; Knowles, P. J. *Chem. Phys. Lett.* **1994**, *227*, 321.

(46) Liu, R.; Zhou, X. *Chem. Phys. Lett.* **1993**, *207*, 185.

(47) Liu, R.; Zhou, X. *J. Phys. Chem.* **1993**, *97*, 9613.

(48) Liu, R.; Zhou, X. *J. Phys. Chem.* **1993**, *97*, 9618.

(49) Chipman, D. M.; Liu, R.; Zhou, X.; Pulay, P. *J. Chem. Phys*. **1994**, *100*, 5023.

(50) (a) Becke, A. D. *J. Chem. Phys.* **1993**, *98*, 5648; (b) **1992**, *96*, 2155; (c) **1992**, *97*, 9173.

(51) Lee, C.; Yang, W.; Parr, R. G. *Phys. Rev.* **1988**, *B37*, 785.

(52) Frisch, M. J.; Trucks, G. W.; Head-Gordon, M.; Gill, P. M. W.; Wong, M. W.; Foresman, J. B.; Johnson, B. G.; Schlegel, H. B.; Robb, M. A.; Replogle, E. S.; Gomperts, R.; Andres, J. L.; Raghavachari, K.; Binkley, J. S.; Gonzales, C.; Martin, R. L.; Fox, D. J.; DeFrees, D. J.; Baker, J.; Stewart, J. J. P.; Pople, J. A. *GAUSSIAN 92/DFT*; Gaussian, Inc.: Pittsburgh, PA, 1993.

(53) MOLPRO is an *ab initio* program for molecular electronic structure calculations written by Werner, H.-J. and Knowles, P. J. with contributions from a number of other people.

(54) Yu, H.; Goddard, J. D. *J. Mol. Struct.* **1991**, *233*, 129.

(55) Qin, Y.; Wheeler, R. A. *J. Chem. Phys.* **1995**, *102*, 1689; *J. Chem. Phys.* **1995**, *102*, 1689.

(56) Gunion, R. F.; Gilles, M. K.; Polak, M. L.; Lineberger, W. C. *Int. J. Mass Spectrom. Ion Processes* **1992**, *117*, 601.

(57) Dupuis, M.; Chin, S.; Marquez, A. CHEM-Station And HONDO. In *Relativistic And Electron Correlation Effects in Molecules and Clusters*; Malli, G. L. Ed.; NATO ASI Series; Plenum Press: New York, 1992. The modification of the algorithm of searching the lowest point of the seam of crossing was due to Dunn, K. M. and Morokuma, K. *J. Chem. Phys.* **1995**, *102*, 4904.

(58) Gonzalez, C.; Schlegel, H. B. *J. Phys. Chem*. **1989**, *90*, 2154.

(59) (a) Marcus, R. A.; Rice, O. K. *J. Phys. Colloid Chem.* **1951**, *55*, 894. (b) Marcus, R. A. *J. Chem. Phys.* **1952**, *20*, 359; (c) **1965**, *43*, 2658; (d) **1970**, *52*, 1018.

(60) Troe, J. *J. Phys. Chem*. **1979**, *83*, 114.

(61) Ahlmeyer, E.; Bich, E.; Opel, G.; Schulze, P.; Vogel, E. *Z. Phys. Chem*. **1982**, *263*, 519.

(62) Hirshfelder, J. O.; Curtiss, C. F.; Bird, R. B. *Molecular Theory of Gases and Liquids*; Wiley: New York, 1954.

(63) Lin, M. C.; Laidler, K. J. *Trans. Faraday Soc*. **1968**, *94*, 64.

JP953566W